Electronic Supplementary Material (ESI) for Dalton Transactions.
This journal is © The Royal Society of Chemistry 2016

Ferromagnetic coupling mediated by Co···π non-covalent contacts in a pentacoordinate Co(II) compound showing field-induced slow relaxation of magnetization

I. Nemec,[a] R. Herchel,[a] and Z. Trávníček[a]*

Content

Selected experimental data for [Co(dpt)(NCS)$_2$]

Synthesis

Synthesis of [Co(dpt)(NCS)$_2$] was performed according to the procedure published by J. Boeckmann et al.[1] Elemental analysis: Mr = 306.3, $C_8H_{17}Co_1N_5S_2$, calculated (in %): C, 31.4; H, 5.6; N, 22.9; found (in %): C, 31.1; H, 5.5, N, 22.6. The zinc diluted sample was prepared in same manner but instead of pure $CoCl_2$ the mixture of $CoCl_2$ and $ZnCl_2$ (in molar ratio 1:9) was used. The phase purity was confirmed by X-ray powder diffraction (Fig. S1, below). The Co^{II} molar fraction was estimated to be 0.14 according to static magnetic measurements.

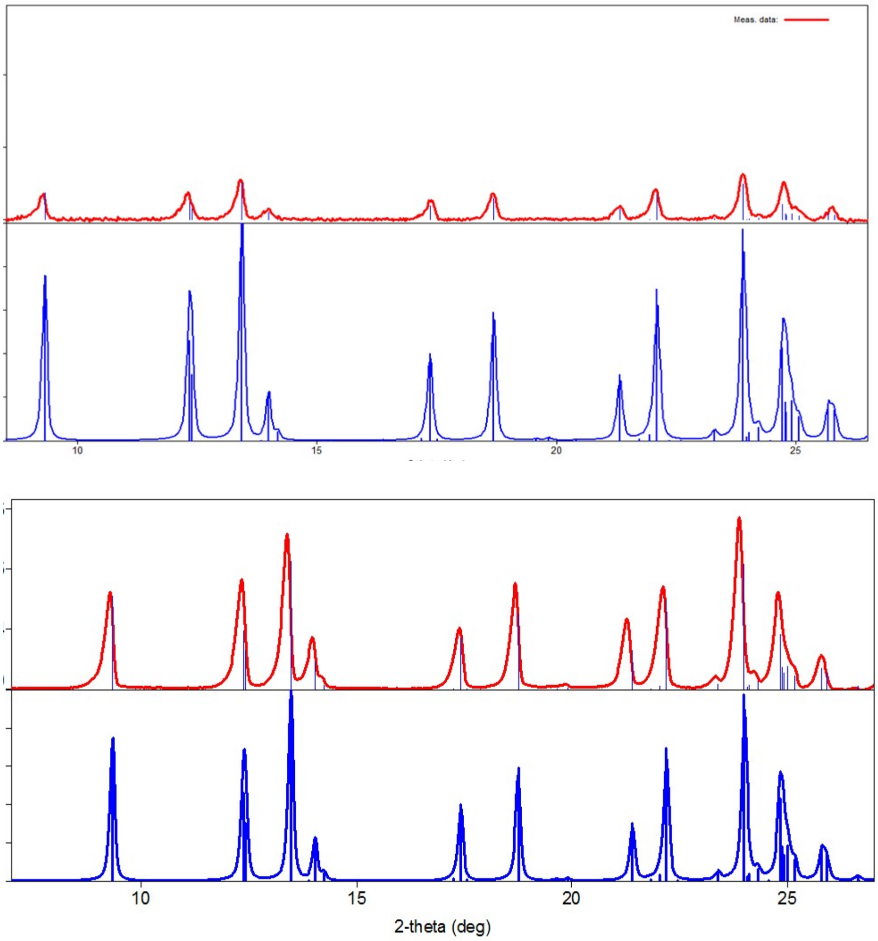

Fig.S1 X-ray powder diffraction pattern for [Co(dpt)(NCS)$_2$] (above) and zinc diluted compound (below). Experimental data are shown as a red line, calculated as a blue line.

Physical methods. Elemental analysis (C, H, N) was performed on a Flash 2000 CHNO-S Analyzer (Thermo Scientific). Temperature dependence of the magnetization at B = 0.1 T from 1.9 to 300 K and the isothermal magnetizations at T = 2.0 and 5.0 K up to B = 5 T were measured using MPMS XL-7 SQUID magnetometer (Quantum Design). The experimental data were corrected for diamagnetism. Measurements of AC susceptibility were carried out in a 3.8 Oe ac field oscillating at various frequencies from 1 to 1500 Hz and with various dc fields. The X-ray powder diffraction patterns of all solid samples were recorded on an MiniFlex600 (Rigaku) instrument equipped with the Bragg−Brentano geometry, and with iron-filtered Cu Kα 1,2 radiation.

Theoretical methods. All theoretical calculations were performed with the ORCA 3.0 computational package.[2] All the calculations employed the scalar relativistic contracted version of def2-TZVP(-f) basis functions[3] together with the zero order regular approximation (ZORA)[4] and also utilizing the chain-of-spheres (RIJCOSX) approximation to exact exchange.[5] DFT calculations were based on B3LYP functional.[6] The ZFS and *g* tensors were calculated by using self-consistent field (SA-CASSCF) wave functions[7] complemented by N-electron valence second order perturbation theory (NEVPT2).[8] The active space of the CASSCF calculation was set to five *d*-orbitals of Co(II) (CAS(7,5)). The ZFS parameters, based on dominant spin−orbit coupling contributions from excited states, were calculated through quasi-degenerate perturbation theory (QDPT),[9] in which approximations to the Breit-Pauli form of the spin-orbit coupling operator (SOMF approximation)[10] and the effective Hamiltonian theory[11] were utilized.

Crystal Structure

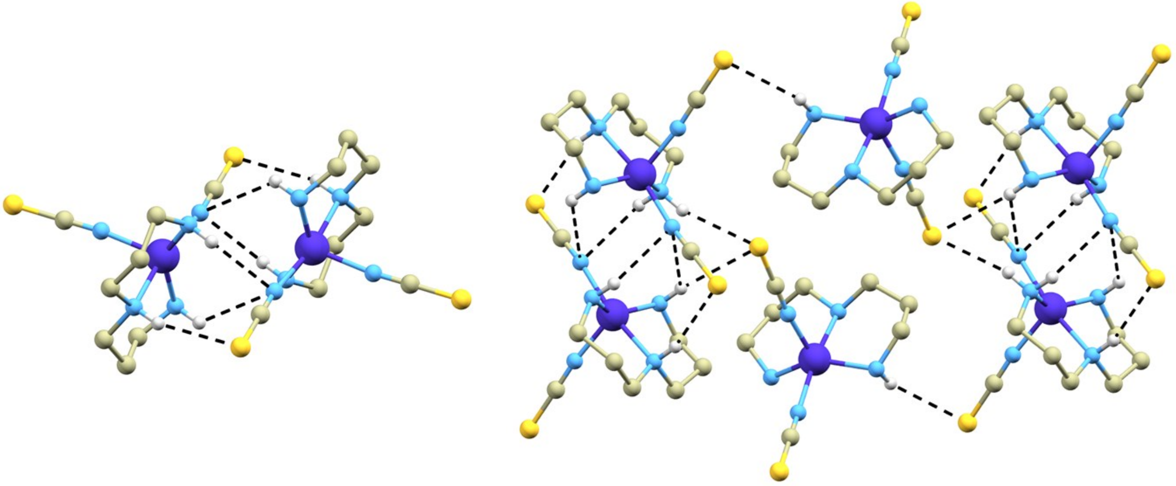

Fig.S2 Hydrogen bonding *Left*: A perspective view on N–H⋯S and N–H⋯π hydrogen bonding in supramolecular dimer [Co(dpt)(NCS)$_2$]$_2$. *Right*: A view on hydrogen bonding in the crystal structure of [Co(dpt)(NCS)$_2$].

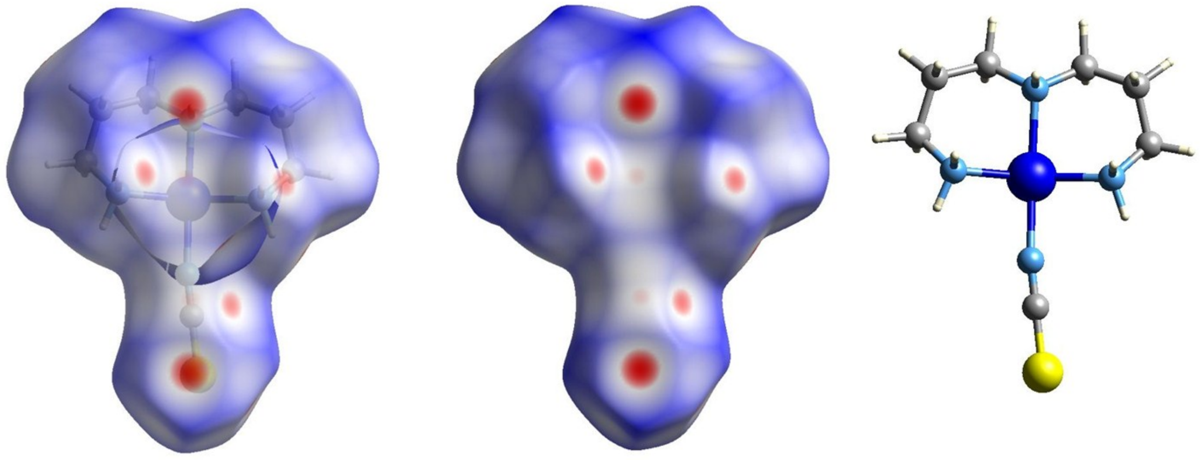

Fig. S3 Calculations of Hirschfield surface mapped with d_{norm} for $[\mathrm{Co(dpt)(NCS)_2}]$ molecule. *Left*: transparent view. *Middle*: full view. *Right*: Orientation of molecule displayed in a ball-stick model. Areas coloured red indicate intermolecular contact.

Magnetic properties

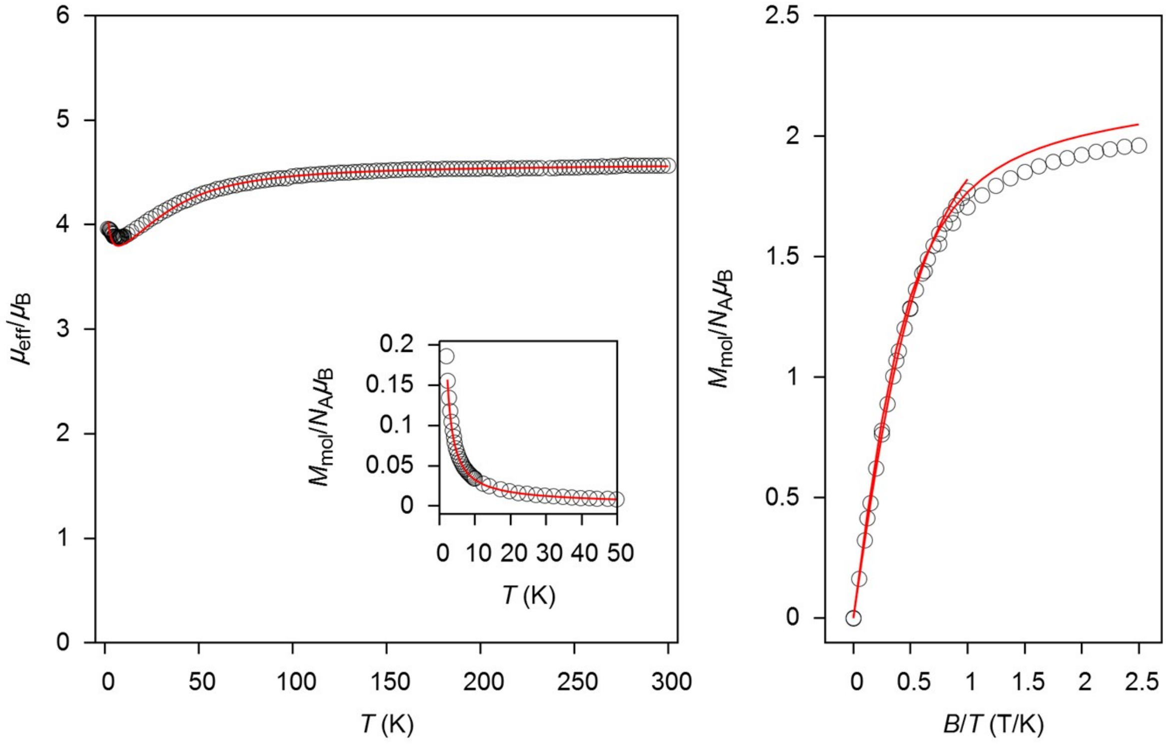

Fig. S4 *Left*: the temperature dependence of the effective magnetic moment and molar magnetization measured at B = 0.1 T. *Right*: the reduced magnetization data measured at T = 2 and 5 K. Empty circles: experimental data. Red full lines: calculated data using eq. 1, with $g = 2.34$, $D = +36.2\ \mathrm{cm^{-1}}$, $E/D = 0.33$ and $\chi_{\mathrm{TIP}} = 2.6\times10^{-9}\ \mathrm{m^3mol^{-1}}$.

CASSCF/NEVPT2 calculations

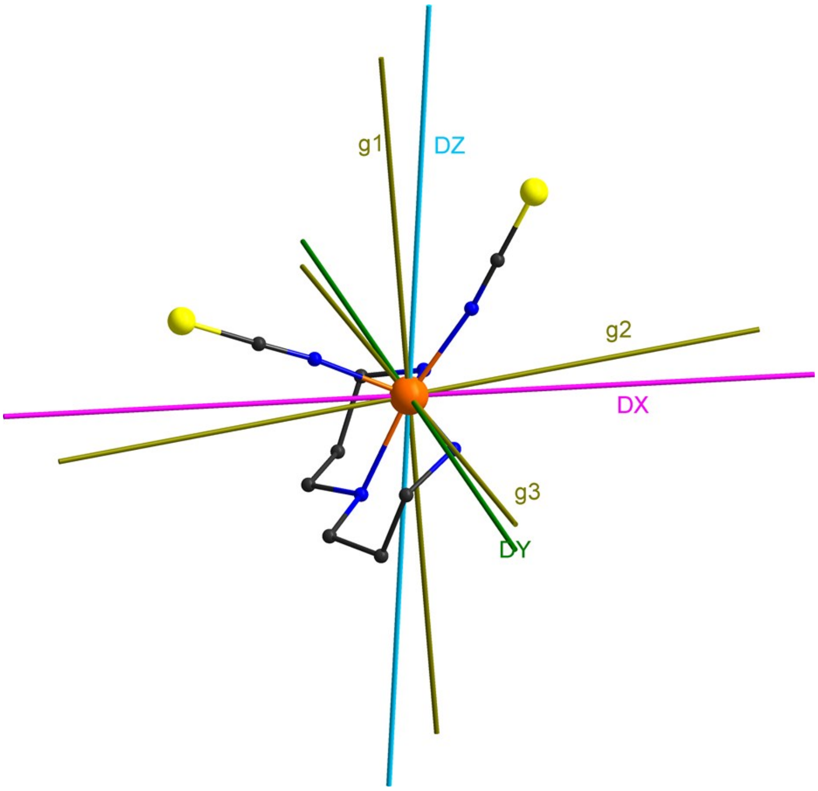

Fig. S5 The molecular structure of 1 overlaid with *g*-tensor and *D*-tensor axes derived with the spin Hamiltonian for S = 3/2, where g_1 = 2.079, g_2 = 2.362, g_3 = 2.497.

X-band EPR

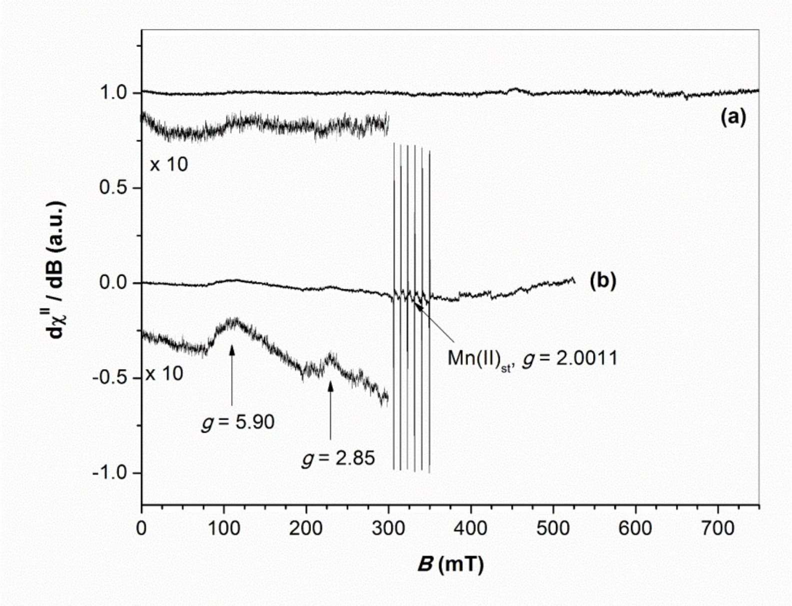

Figure 1. EPR spectra: **(a)** Frequency of 9.1608 GHz, modular frequency of 100 KHz, modular width of 1.00 mT, sweep time 8 min, time const. 0.03 s, microwave power of 2.00 mW, T = 110 K. **(b)** Same sample but recorded with the concomitant presence of Mn(II) standard as second separate probe in the cavity resonator. Frequency of 9.1604 GHz, modular frequency of 100 KHz, modular width of 1.00 mT, sweep time 8 min, time const. 0.03 s, microwave power of 2.40 mW, T = 110 K.
*Note that differing from spectrum **(a)** that appears EPR silent consistent with the hypothesis of large axial ZFS, when slightly higher microwave power is applied to the sample (**b spectrum**) the presence of resolved component encoding the g-anisotropy (g-values shown) appeared.*

DFT calculations

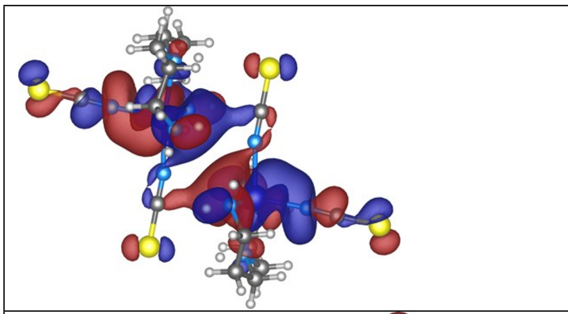	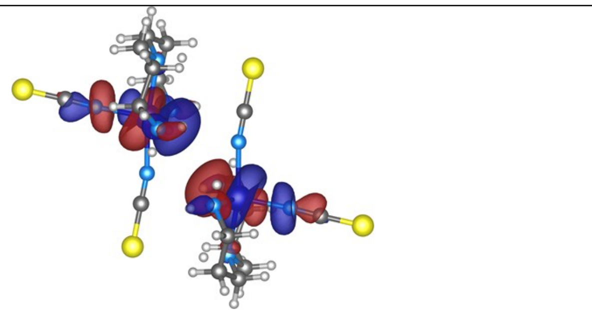	$S_{\alpha\beta}$ = 0.00968
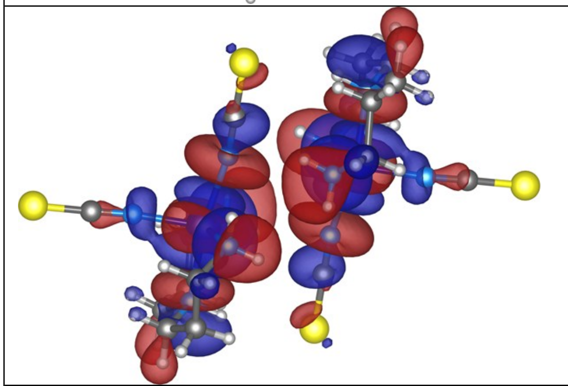	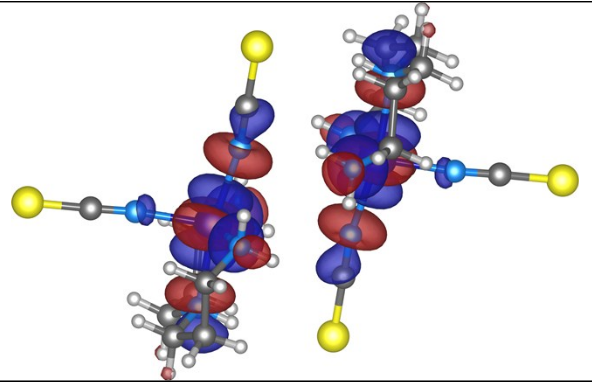	$S_{\alpha\beta}$ = 0.00429
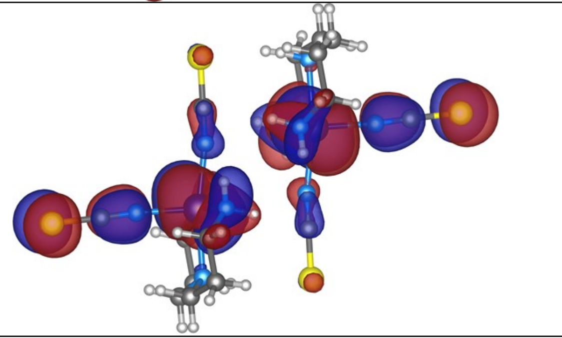	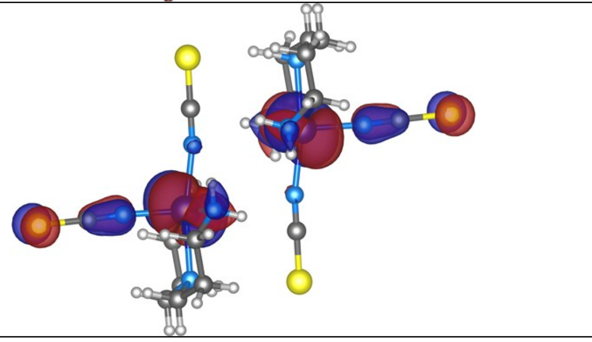	$S_{\alpha\beta}$ = 0.00104

Fig. S7 The non-orthogonal magnetic orbitals of the broken-symmetry spin state with the given overlap ($S_{\alpha\beta}$) visualized for [{Co(dpt)(NCS)$_2$}$_2$]of **1** as derived from B3LYP/ZORA/def2-TZVP(-f) calculations. The two columns correspond to different isosurface levels.

Magnetic properties of a Zn diluted sample (1-Zn)

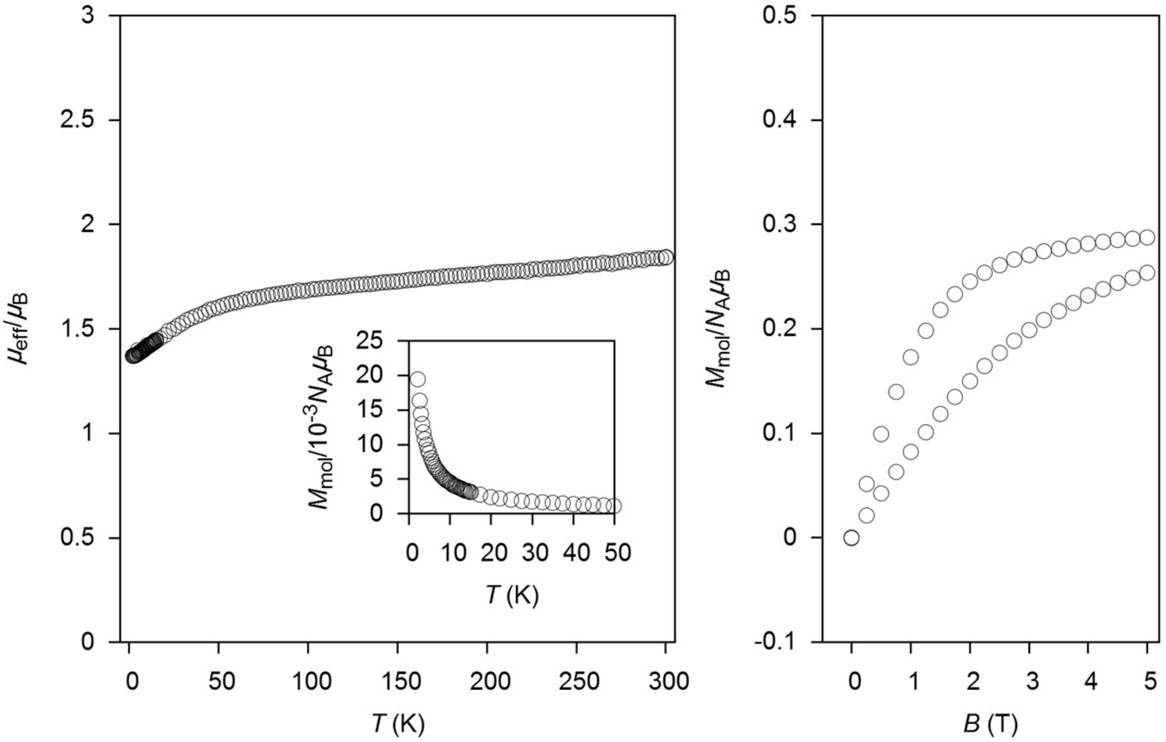

Fig. S8 Magnetic data for 1-Zn. ***Left:*** the temperature dependence of the effective magnetic moment and molar magnetization measured at B = 0.1 T. *Right*: the magnetization data measured at T = 2 and 5 K.

Table S1. Parameters of one-component Debye model for **1** derived according Eq. 2 in main text.

T/K	χ_S/(10^{-6} m^{3}mol^{-1})	χ_T/(10^{-6} m^{3}mol^{-1})	α	τ/(10^{-2} s)
1.90	7.538	9.769	0.304	2.792
2.20	6.865	9.085	0.339	3.619
2.50	6.247	8.097	0.378	2.797
2.80	5.869	7.272	0.284	1.685
3.10	5.483	6.705	0.384	1.585
3.40	5.174	6.134	0.378	1.236
3.70	4.884	5.656	0.373	1.097
4.00	4.689	5.263	0.394	1.151
4.30	4.478	4.900	0.477	1.538

Table S2. Parameters of one-component Debye model for **1-Zn** derived according Eq. 2 in main text.

T/K	χ_S/(10^{-6} m^{3}mol^{-1})	χ_T/(10^{-6} m^{3}mol^{-1})	α	τ/(10^{-4} s)
1.90	0.156	1.338	0.123	5.626
2.10	0.146	1.228	0.129	5.232
2.30	0.167	1.136	0.115	4.848
2.50	0.156	1.063	0.128	4.468
2.70	0.112	0.992	0.150	3.643
2.90	0.128	0.927	0.113	3.914
3.10	0.139	0.860	0.107	3.545
3.30	0.130	0.823	0.102	3.203
3.50	0.117	0.797	0.106	2.966
3.70	0.053	0.747	0.192	2.075
3.90	0.097	0.700	0.088	2.084
4.10	0.100	0.672	0.066	1.926

---

[1] J. Boeckmann and C. Nather, *Acta Cryst. Sec. E*, 2011, 67, m1025-m1026.

[2] F. Neese, WIREs Comput. Mol. Sci. 2012, **2**, 73-78.

[3] D. A. Pantazis, X.-Y. Chen, C. R. Landis and F. Neese, *J. Chem. Theory Comput.*, 2008, **4**, 908-919.

[4] (a) E. Vanlenthe, E. J. Baerends and J. G. Snijders, *J. Chem. Phys.*, 1993, **99**, 4597-4610. (b) C. van Wullen, *J. Chem. Phys.*, 1998, **109**, 392-399.

[5] F. Neese, F. Wennmohs, A. Hansen and U. Becker, *Chem. Phys.*, 2009, **356**, 98-109.

[6] (a) C. Lee, W. Yang and R. G. Parr, *Phys. Rev. B: Condens. Matter*, 1988, **37**, 785; (b) A. D. Becke, *J. Chem. Phys.*, 1993, **98**, 1372; (c) A. D. Becke, *J. Chem. Phys.*, 1993, **98**, 5648; (d) P. J. Stephens, F. J. Devlin, C. F. Chabalowski and M. J. Frisch, *J. Phys. Chem.*, 1994, **98**, 11623.

[7] P. A. Malmqvist and B. O. Roos, *Chem. Phys. Lett.*, 1989, **155**, 189-194.

[8] (a) C. Angeli, R. Cimiraglia, S. Evangelisti, T. Leininger and J. P. Malrieu, *J. Chem. Phys.*, 2001, **114**, 10252-10264. (b) C. Angeli, R. Cimiraglia and J. P. Malrieu, *Chem.Phys. Lett.*, 2001, **350**, 297-305. (c) C. Angeli, R. Cimiraglia and J. P. Malrieu, *J. Chem. Phys.*, 2002, **117**, 9138-9153. (d) 1. C. Angeli, S. Borini, M. Cestari and R. Cimiraglia, *J. Chem. Phys.*, 2004, **121**, 4043-4049. (e) C. Angeli, B. Bories, A. Cavallini and R. Cimiraglia, *J. Chem. Phys.*, 2006, **124**, 054108.

[9] D. Ganyushin and F. Neese, *J. Chem. Phys.*, 2006, **125**, 024103.

[10] F. Neese, *J. Chem. Phys.*, 2005, **122**, 034107.

[11] R. Maurice, R. Bastardis, C. de Graaf, N. Suaud, T. Mallah and N. Guihéry, *J. Chem. Theory Comput.*, 2009, **5**, 2977-2984.